

Spin-resolved Mott crossover and entanglement in the half-filled Hubbard model

Md Fahad Equbal * and M. A. H. Ahsan [†]

Department of Physics, Jamia Millia Islamia (Central University), New Delhi 110025, India

(Dated: December 2, 2025)

We study interaction-driven crossover from a correlated metallic state to Mott-insulating state on the half-filled 3×3 square cluster using exact diagonalization in the $S = 1/2$ and $S = 3/2$ sectors. Using complementary diagnostics such as order parameters, principal component analysis (PCA) of correlation matrices and quantum geometry, we obtain a unified, data-driven characterization of the crossover. All three diagnostics consistently identify a broad crossover centered in the weak-to-intermediate coupling regime $U \approx 2 - 6$; charge gaps open rapidly, double occupancy suppresses, local moments form, entanglement is significantly reduced, PCA concentrates variance into a few dominant modes and the distance matrices reveals rapid wavefunction reorganization. Our multi-pronged approach establishes the Mott crossover as a smooth but well defined reorganization of electronic correlations with pronounced spin-sector dependence in finite systems.

Keywords: Mott crossover; Entanglement entropy; Principal component analysis; Quantum geometry; Hubbard model; Exact diagonalization

Introduction.—The interaction-driven crossover from an itinerant metal to Mott insulator [1], remains one of the most fundamental and actively studied phenomena in strongly correlated electron systems. While the thermodynamic limit of this crossover has been extensively investigated through dynamical mean-field theory [2] and other many-body approaches, the behavior of finite quantum clusters presents unique challenges and opportunities for understanding the microscopic mechanisms driving correlation-induced localization. Recent experimental advances in quantum simulations [3] and two-dimensional (2D) materials [4, 5] have further highlighted the importance of understanding correlation physics in confined geometries where finite-size effects and spin frustration play crucial roles [6].

Traditional approaches in characterizing the Mott crossover have relied heavily on order parameters such as charge gaps and double occupancy [7]. However, the advent of machine learning techniques in quantum physics [8–10] and quantum information perspectives [11–13] has opened new avenues for identifying and characterizing correlation-driven crossovers. Principal component analysis (PCA) has emerged as a powerful unsupervised learning method for extracting dominant correlation patterns [14], while quantum geometric approaches [15] offer wavefunction based diagnostics of state reorganization. Despite these advances, a comprehensive framework integrating conventional order parameters with modern data-driven and geometric perspectives remains largely unexplored, particularly regarding spin-sector dependence in finite systems.

In this work, we bridge this gap by presenting a multifaceted investigation of the Mott crossover in the half-filled 3×3 square cluster, systematically comparing $S = 1/2$ and $S = 3/2$ spin sectors to uncover spin-dependent signatures of correlation reorganization. Our integrated approach combines spin-resolved charge gaps, local observables, and entanglement entropy with PCA of correlation matrices and quantum distance matrices, providing complementary perspectives that collectively sharpen the iden-

tification of the crossover regime. The recent work by Chatzieftheriou et al. [5] on local and nonlocal correlations in the 2D Hubbard model and the analysis of rare-earth nickelates on the origin of metal-insulator transitions [16] underscores the importance of such integrated diagnostic frameworks when approaching the Mott problem, while studies on entanglement [11, 12] and quantum geometry [15] provide the theoretical foundation for our investigations.

Hubbard model.—The Hamiltonian for one-band Hubbard model [17] in real space is written as

$$H = -t \sum_{\langle ij \rangle \sigma} (c_{i\sigma}^\dagger c_{j\sigma} + c_{j\sigma}^\dagger c_{i\sigma}) + U \sum_i n_{i\uparrow} n_{i\downarrow}, \quad (1)$$

where $c_{i\sigma}^\dagger (c_{i\sigma})$ is the fermionic operator that creates (annihilates) an electron with spin $\sigma \in \{\uparrow, \downarrow\}$ at lattice site i , and $\langle ij \rangle$ denotes nearest neighbors (NN) sites on the lattice. The parameters t and U represent the NN hopping matrix amplitude and the on-site Coulomb interaction, respectively. The number operator $n_{i\sigma} = c_{i\sigma}^\dagger c_{i\sigma}$ counts particles at site i with spin σ . The tight-binding dispersion relation corresponding to non-interacting ($U = 0$) case in 2D is given by $\epsilon_k = -2t(\cos k_x + \cos k_y)$, with a bandwidth $W = 8t$. Throughout, this work, we have set the energy scale $t = 1$.

We employ exact diagonalization (ED) to compute ground and low-lying excited states on finite-size cluster. ED provides complete access to all correlation functions, making it ideal for testing data-driven analysis methods despite its limited system size. We choose a minimal 3×3 square cluster with open boundary conditions and exploit spin-rotational symmetry to construct spin-adapted basis [18], which significantly reduces the Hilbert space dimensionality.

Results and discussion.—To elucidate the evolution of the ground state across the interaction-driven crossover from the metallic to the Mott-insulating regime on the 3×3 Hubbard cluster, we combine conventional order-parameter diagnostics with modern correlation-matrix analysis and quantum-geometric probes. Throughout, we track the system in both the $S = 1/2$ and $S = 3/2$ sectors at half filling to reveal possible spin-sector dependent signatures

* md179654@st.jmi.ac.in

[†] mahsan@jmi.ac.in

of localization. We first examine spin-resolved charge gaps and local observables such as double occupancy, local moments, and the von-Neumann entanglement entropy to establish the microscopic indicators of the crossover. We then employ principal component analysis (PCA) of charge-charge and spin-spin correlation matrices to reveal the dominant correlation modes and their sector-dependent evolution with U . Finally, we quantify the sensitivity of the many-body wavefunction to interaction tuning via quantum geometry distance matrices, providing a complementary quantum-geometry perspective that sharpens the identification of the crossover region and highlights its finite-size and spin-sector manifestations.

Spin-resolved charge gap.—To quantify the spin-dependent incompressibility of the half-filled Hubbard cluster, we investigate the spin-resolved charge gap $\Delta_c(S)$ by tracking the lowest-energy states across particle-number sectors constrained to a fixed total-spin manifold. Denoting the ground-state energy with N electrons and total spin S by $E(N, S)$, the charge gap for an excitation channel characterized by S_N (for $N = 9$) and $S_{N\pm 1}$ (for $N = 8, 10$) is defined as

$$\Delta_c(S_N) = E(10, S_{N+1}) + E(8, S_{N-1}) - 2E(9, S_N), \quad (2)$$

with $(S_{N-1}, S_N, S_{N+1}) = (0, \frac{1}{2}, 0)$ defining the low-spin channel and $(1, \frac{3}{2}, 1)$ defining the high-spin channel. These spin-resolved gaps provide a controlled measure of how charge addition and removal processes reorganize spin correlations in the strongly interacting regime, thereby allowing us to disentangle the spin-charge entanglement that underpins the Mott crossover.

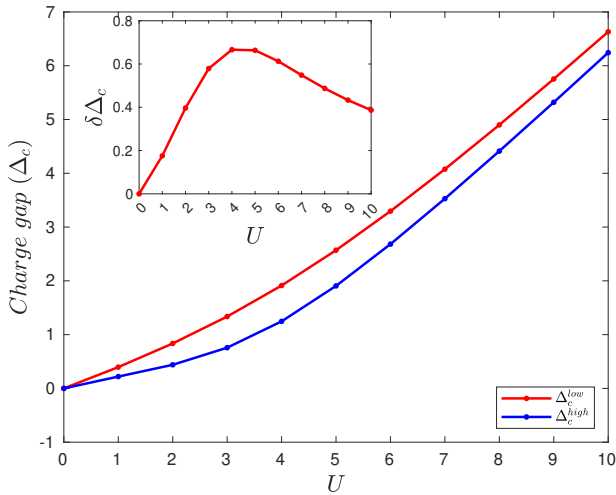


FIG. 1. Spin-resolved charge gaps as a function of U on the 3×3 square cluster. The low-spin gap $\Delta_c^{low} = E(10, 0) + E(8, 0) - 2E(9, \frac{1}{2})$ and the high-spin gap $\Delta_c^{high} = E(10, 1) + E(8, 1) - 2E(9, \frac{3}{2})$ both increase monotonically with U , reflecting the suppression of charge fluctuations. The low-spin sector remains consistently more gapped across the full range of interactions. Inset: The gap difference $\delta\Delta_c = \Delta_c^{low} - \Delta_c^{high}$ highlights a pronounced maximum at intermediate U , indicating a non-trivial spin-dependent crossover in the charge-excited sector.

Figure 1 shows the evolution of low-spin charge gap Δ_c^{low} and high-spin charge gap Δ_c^{high} as a function of the on-site

repulsion U . Both spin sectors exhibit a monotonic growth of the charge gap with increasing interaction strength, consistent with the progressive suppression of charge fluctuations characteristic of a Mott insulating state. In the non-interacting limit ($U = 0$), both Δ_c^{low} and Δ_c^{high} is zero, but they split rapidly for $U \geq 1$, reflecting the enhanced energetic cost associated with promoting the system into spin-polarized charge excitation channels. Across the full interaction regime, the low-spin gap remains systematically larger, indicating that the background singlet correlations are more resilient against charge rearrangements than their high-spin counterparts. The inset displays the gap difference $\delta\Delta_c = \Delta_c^{low} - \Delta_c^{high}$, which provides a sharp diagnostic of the crossover in the spin structure of charge excitations. Notably, $\delta\Delta_c$ increases between $U \approx 1$ and $U \approx 4$, reaching a pronounced maximum around intermediate coupling. This behavior signals a non-trivial reorganization of spin correlations in the charge-defected sector: while both gaps increase, the high-spin excitation gains relative stability in the crossover region, pointing to a competition between short-range singlet physics and emerging high-spin configurations. For larger U , $\delta\Delta_c$ gradually decreases, consistent with the asymptotic alignment of spin energy scales in the strong-coupling limit where the cost of charge fluctuations dominates the residual spin dependence.

Local observables: local moment and double occupancy.—To probe the formation of local magnetic moments and the suppression of charge fluctuations across the interaction-driven crossover, we compute the average local moment $\bar{m} = \frac{4}{N} \sum_i \langle (n_{i\uparrow} - n_{i\downarrow})^2 \rangle$ and the average double occupancy $\bar{d} = \frac{M}{N^2} \sum_i \langle n_{i\uparrow} n_{i\downarrow} \rangle$, where M represents number of sites with N electrons. At half-filling $N = M$. These local observables quantify the degree of spin polarization and on-site charge pairing.

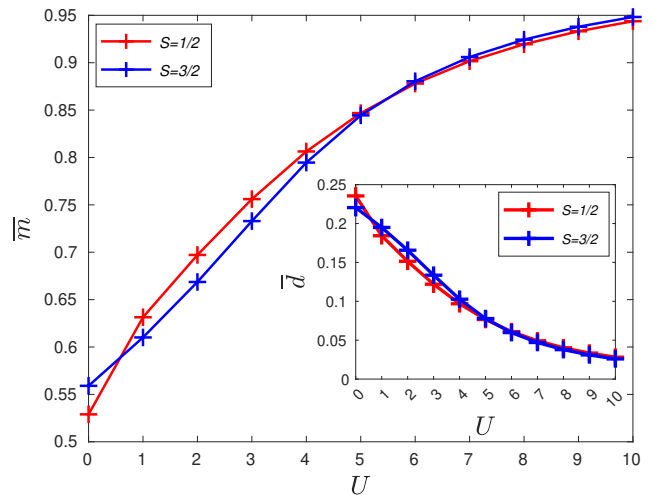


FIG. 2. Average local moment \bar{m} (main panel) and average double occupancy \bar{d} (inset) as a function of U for the half-filled 3×3 square cluster in the $S = 1/2$ and $S = 3/2$ sectors. The rapid decrease of \bar{d} at weak-intermediate U and the monotonic growth of \bar{m} signal the loss of on-site charge fluctuations and the concomitant formation of robust local moments.

Figure 2 displays \bar{m} (main panel) and \bar{d} (inset) for the half-filled 3×3 square cluster in the $S = 1/2$ and $S = 3/2$

sectors for $U = 0 - 10$. The double occupancy falls rapidly from $\bar{d} \approx 0.2355$ (at $U = 0$) to $\bar{d} \approx 0.0281$ (at $U = 10$) in the $S = 1/2$ sector (with almost identical values for $S = 3/2$), indicating strong suppression of on-site charge fluctuations at large U . Concurrently, the average local moment grows monotonically from $\bar{m} \approx 0.53$ to $\bar{m} \approx 0.94$ ($S = 1/2$) and from $\bar{m} \approx 0.56$ to $\bar{m} \approx 0.95$ ($S = 3/2$), demonstrating the progressive formation of well-defined moments.

Two observations are noteworthy. First, the most rapid change in \bar{d} occurs at weak to intermediate coupling (roughly $U \lesssim 4$), mirroring the region where the charge gap grows steeply—this concordance supports interpreting the behavior as a crossover toward Mott localization rather than a sharp finite-size transition. Second, spin-sector differences are small but systematic: \bar{d} is marginally lower and \bar{m} marginally higher in the $S = 3/2$ sector at small U , and the two sectors converge closely at large U . This indicates that spin polarization slightly disfavors double occupancy and promotes larger instantaneous moments at weak coupling, while in the strong-coupling limit the interaction energy dominates and the spin-sector dependence of these local observables becomes negligible.

von-Neumann entanglement entropy.—To further quantify the interaction-driven crossover and its imprint on many-body quantum correlations, we compute the bipartite von-Neumann entanglement entropy from the full ground-state wave function $|\psi_0\rangle$ in both the $S = 1/2$ and $S = 3/2$ sectors. We partition the 3×3 square cluster into two complementary sublattices A and B , and obtain the reduced density matrix of subsystem A by tracing out the degrees of freedom of B :

$$\rho_A = \text{Tr}_B(|\psi_0\rangle\langle\psi_0|). \quad (3)$$

The entanglement entropy is then given by the standard von-Neumann measure

$$S_A = -\text{Tr}(\rho_A \log_2 \rho_A), \quad (4)$$

which captures how the ground state redistributes quantum information between the two spin-resolved sectors and directly encodes the growth of many-body correlations associated with the Mott crossover.

Figure 3 shows the von-Neumann entanglement entropy S_A as a function of U , computed for the bipartition $A \cup B$ in the half-filled 3×3 square cluster for the $S = 1/2$ and $S = 3/2$ sectors. At $U = 0$, both sectors exhibit a large entanglement entropy ($S_A \approx 5.46$ for $S = 1/2$ and $S_A \approx 5.37$ for $S = 3/2$), reflecting the strongly delocalized, metallic-like ground state with substantial charge fluctuations across the bipartition. As U increases, S_A decreases monotonically, dropping to $S_A \approx 2.76$ ($S = 1/2$) and $S_A \approx 2.98$ ($S = 3/2$) at $U = 10$; this decay signals the progressive suppression of inter-sublattice quantum correlations and the emergence of quasi-localized spins characteristic of Mott physics.

Two systematic features stand out. First, the rate of entanglement suppression is most pronounced for $U \lesssim 4$, precisely the regime where the charge gap grows rapidly (Fig. 1) and where \bar{d} collapses toward zero (Fig. 2), indicating that the crossover is driven by the quenching of charge fluctuations. Second, the $S = 3/2$ sector consistently maintains a higher entanglement entropy than the $S = 1/2$ sector at intermediate and large U . This subtle but robust

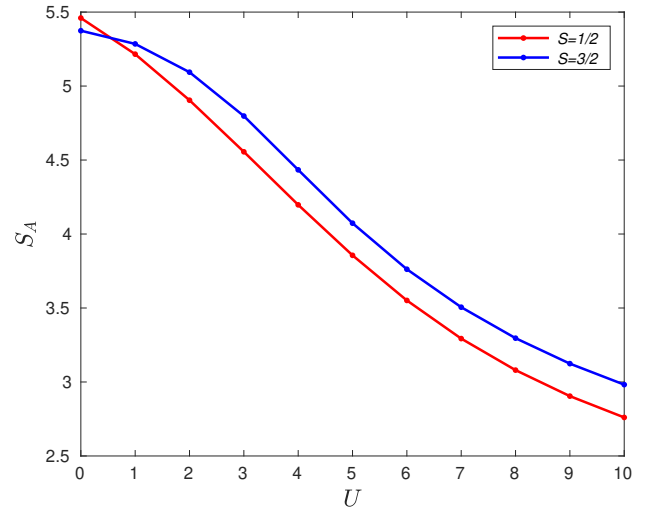


FIG. 3. von-Neumann entanglement entropy S_A as a function of the interaction strength U for the half-filled 3×3 square cluster in the $S = 1/2$ and $S = 3/2$ spin sectors. Both sectors exhibit large entanglement at $U = 0$, indicative of strong inter-sublattice charge fluctuations; S_A decreases monotonically with U , reflecting the suppression of quantum correlations and the buildup of local moments.

offset reflects the enhanced spin configurational space available to the partially polarized background, even as charge fluctuations are strongly suppressed. In the large U limit, the entanglement approaches a sector-dependent plateau, consistent with the dominance of superexchange-mediated spin correlations in the effective Heisenberg regime ($J = 4t^2/U$).

Taken together, the monotonic reduction in spin-sector-resolved S_A provides a clear entanglement-based signature of the interaction-driven crossover, complementing the charge-gap and local-moment diagnostics and offering a quantum-information perspective on Mott localization.

PCA of charge and spin correlations.—To gain a data-driven, unsupervised view of how electronic correlations reorganize across the metallic to Mott insulator crossover regime, we perform principal component analysis (PCA) of the site-resolved charge and spin correlation matrices. This machine-learning technique allows us to cut through the complexity of the full correlation data and identify the dominant, collective fluctuation modes that emerge as a function of the Hubbard interaction U . For a given $M \times M$ correlation matrix, the data are first centered by subtracting the mean of each row. The covariance matrix is then constructed as $C = \frac{1}{M} X^T X$. Diagonalization of C yields eigenvalues λ_k and orthonormal eigenvectors w_k via $Cw_k = \lambda_k w_k$, where each w_k defines a principal component corresponding to an independent fluctuation mode. The normalized explained variance-ratio, $\tilde{\lambda}_k = \frac{\lambda_k}{\sum_i \lambda_i}$, quantifies the statistical importance of each component and serves as the primary diagnostic in our analysis. In practice, the leading variance-ratios $\tilde{\lambda}_k$ reveal which fluctuation channels dominate the correlation data. By tracking their evolution with the interaction strength U , we can identify charge-dominated or spin-dominated regimes in a

fully data-driven manner. This unsupervised approach thus complements traditional observables and provides a transparent framework for visualizing correlation reorganization and crossovers in finite-size Hubbard clusters.

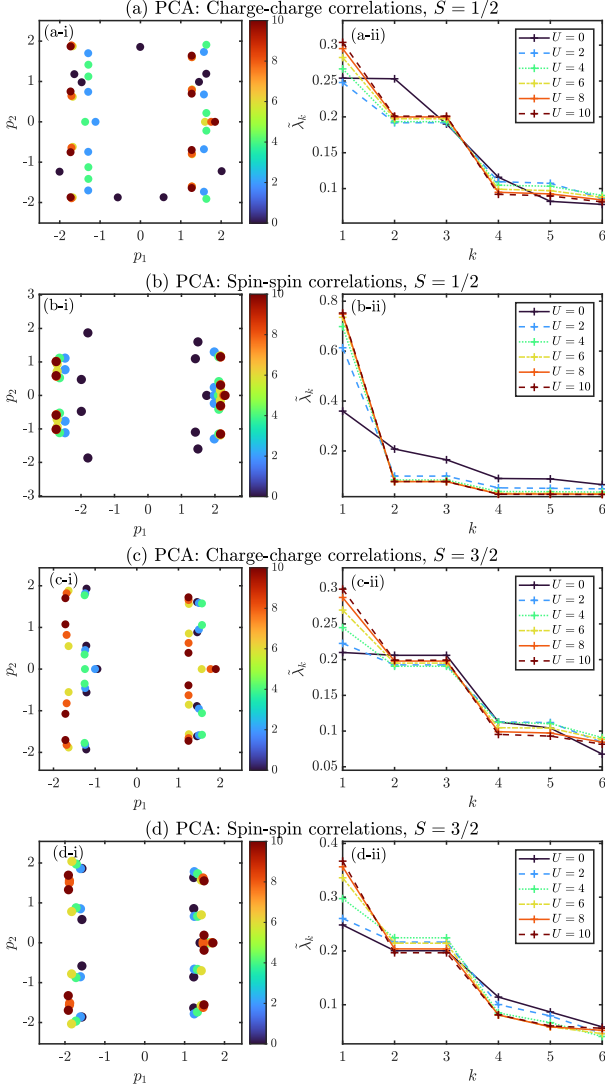


FIG. 4. Principal component analysis (PCA) of (a,c) charge correlation functions and (b,d) spin correlation functions, in $S = 1/2$ and $S = 3/2$ sectors, respectively for the half-filled band of 3×3 square cluster. Panels (a-i), (b-i), (c-i) and (d-i) show the projection of the correlation data onto the space of the first two principal components (p_1, p_2) for $U = 0, 2, 4, 6, 8$ and 10 with colors representing the on-site interaction U . Panels (a-ii), (b-ii), (c-ii) and (d-ii) display the explained variance-ratio $\tilde{\lambda}_k$ of the first six principal components as functions of the component index k .

Figure 4 presents the PCA results for the half-filled 3×3 cluster, with projections onto the first two principal components (left panels) and the explained variance-ratios $\tilde{\lambda}_k$ (right panels) for both $S = 1/2$ and $S = 3/2$ sectors. In the charge sector ($S = 1/2$), the explained variance-ratio of the leading component $\tilde{\lambda}_1$ increases monotonically from 0.2540 ($U = 0$) to 0.3039 ($U = 10$), while the variance becomes increasingly concentrated in the first three components. This evolution reflects the progressive organization

of charge fluctuations into fewer dominant modes as the system transitions from metallic delocalization to Mott localization. The projection plot shows a systematic expansion along the p_1 axis with increasing U , indicating the growing dominance of this primary charge fluctuation channel. The spin sector ($S = 1/2$) exhibits a more dramatic reorganization, with $\tilde{\lambda}_1$ surging from 0.3597 to 0.7527 over the same interaction range. This extraordinary concentration of variance in a single principal component signifies the emergence of a dominant antiferromagnetic fluctuation mode, consistent with the formation of short-range singlet correlations. The projection data collapses dramatically along p_1 with increasing U , visually confirming the dominance of this collective spin mode in the strongly correlated regime. Notably, the spin-sector dependence reveals crucial differences in correlation hierarchy. While both sectors show similar charge PCA evolution, the $S = 3/2$ spin sector maintains significantly more distributed variance ($\tilde{\lambda}_1$ reaches only 0.3670 at $U = 10$) compared to the $S = 1/2$ case. This persistence of multiple competing spin fluctuation modes in the high-spin manifold reflects the frustrated nature of spin configurations in the partially polarized background, where the absence of strong singlet formation preserves a broader spectrum of spin correlations. The most rapid reorganization in both charge and spin variance spectra occurs precisely in the intermediate coupling regime ($U \approx 2 - 6$), coinciding with the crossover region identified by traditional order parameters. This concordance validates the PCA approach as an unbiased diagnostic of the Mott crossover, capturing the fundamental restructuring of correlation modes without a priori assumptions about the nature of the emergent phases.

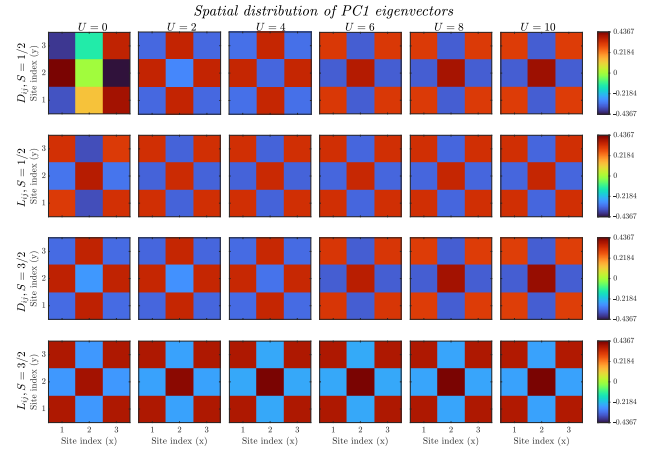


FIG. 5. Spatial distribution of the leading PCA eigenvectors (PC1) for charge (D_{ij}) and spin (L_{ij}) correlation matrices in the $S = 1/2$ and $S = 3/2$ sectors of the half-filled 3×3 Hubbard cluster. Each 3×3 panel shows the normalized eigenvector amplitudes across lattice sites for increasing $U = 0-10$. Charge eigenvectors evolve from inhomogeneous metallic patterns to stabilized checkerboard textures, while spin eigenvectors develop pronounced staggered antiferromagnetic character, especially in the $S = 1/2$ sector, signaling the real-space onset of Mott localization.

To gain microscopic insight into the collective modes identified by PCA, we visualize the spatial structure of

the leading principal component (PC1) eigenvectors for both charge and spin correlation matrices in the $S = 1/2$ and $S = 3/2$ sectors (Fig. 5). These eigenvectors encode the dominant fluctuation patterns that account for the largest share of correlation variance, thereby revealing how real-space correlations reorganize across the Mott crossover regime. In the non-interacting limit ($U = 0$), the charge-sector eigenvectors (D_{ij}) display strong spatial inhomogeneity and alternating sign amplitudes, reflecting delocalized charge fluctuations and metallic coherence across the cluster. As U increases, this pattern rapidly stabilizes into a nearly uniform checkerboard structure of alternating signs, signifying the suppression of charge delocalization and the emergence of localized charge configurations. The spin-sector eigenvectors (L_{ij}) exhibit an even clearer transition: with increasing U , they evolve from disordered amplitude distributions into robust staggered antiferromagnetic patterns, indicating the buildup of short-range magnetic correlations characteristic of the Mott regime. Comparison between the two spin sectors reveals a systematic difference. In the $S = 1/2$ manifold, both charge and spin PC1 maps exhibit strong, spatially ordered alternations consistent with dominant singlet-like correlations, whereas in the $S = 3/2$ manifold, the corresponding eigenvectors remain more diffuse with reduced amplitude contrast, reflecting persistent spin frustration and weaker staggered ordering in the partially polarized background. Together, these spatial patterns provide a direct visualization of how the primary fluctuation channels evolve from delocalized metallic correlations to localized charge and spin order as U drives the system into the Mott regime.

Quantum geometry distance matrix.—To complement our order parameter and PCA analyses with a wavefunction based viewpoint, we adopt the quantum geometry distance matrix formalism introduced by Hassan *et al.* [15], as a diagnostic of the metal-insulator crossover. We form a quantum geometry distance matrix from expectation values of exchange operators that swap the occupation of two single-particle modes. For a normalized many-body ground state $|\psi_0\rangle$, the (squared) quantum overlap associated with exchanging the occupations of modes i and j is $\langle\psi_0|\hat{E}_{ij}|\psi_0\rangle$, and the corresponding distance is defined as

$$d_{ij} = \sqrt{1 - |\langle\psi_0|\hat{E}_{ij}|\psi_0\rangle|^2}, \quad (5)$$

which satisfies the metric properties. For the spinful Hubbard model we employ an exchange operator that acts on the site-orbital degrees of freedom while including spin: in practice we evaluate the expectation of the operator that exchanges the occupation of sites i and j for both spin species. This choice yields a distance matrix that is sensitive to the combined charge-spin coherence between sites; one can readily form spin-resolved variants by restricting the exchange to a single spin projection if desired.

The distance matrices shown in Fig. 6 display a clear geometric signature of the metallic to Mott crossover. In the metallic limit ($U = 0$) the matrix shows pronounced off-diagonal structure and reduced distances among specific site pairs — a direct manifestation of extended intersite coherence and mode clustering. As U increases the off-diagonal elements systematically grow (distance increases) and the matrix becomes progressively diagonally

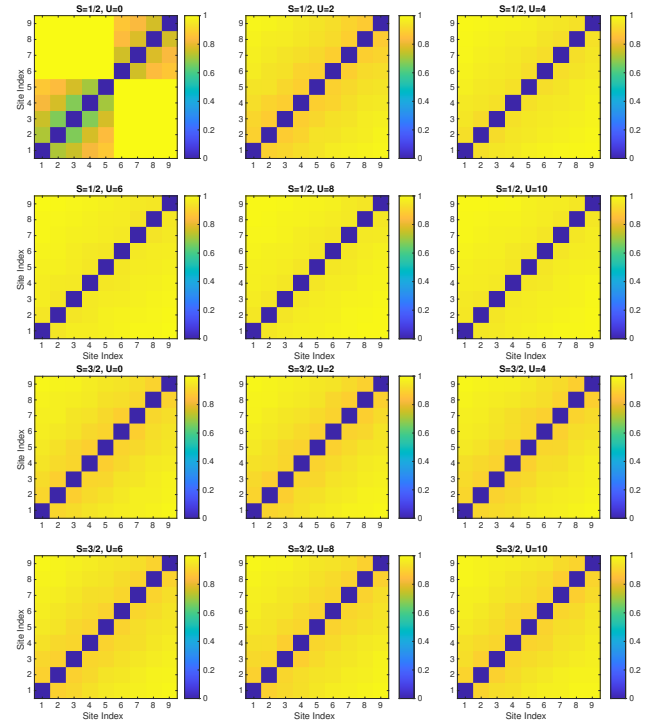


FIG. 6. Distance matrices for the half-filled 3×3 square cluster in spin sectors $S = 1/2$ (top two rows) and $S = 3/2$ (bottom two rows) at representative interaction strengths $U=0, 2, 4, 6, 8$, and 10 . Increasing diagonal dominance with U reflects the progressive localization of electronic states across the Mott crossover regime.

dominated, indicating that local components of the many-body wavefunction decouple from one another and electronic states become localized. Comparing spin sectors, the $S = 1/2$ manifold exhibits larger initial off-diagonal modulation and a sharper evolution toward diagonal dominance than the $S = 3/2$ sector; the latter remains comparatively more uniform at intermediate U , reflecting the reduced intersite coherence in the partially polarized background. Quantitatively, the largest change in the intersite distances occurs in the same weak-to-intermediate coupling regime ($U \approx 2 - 6$) identified by the local observables and PCA, thereby providing a wavefunction based geometric confirmation of the Mott crossover.

Summary and conclusion.—In this work, we have presented a comprehensive analysis of the Mott metal-insulator crossover in the half-filled 3×3 square cluster by examining a suite of complementary diagnostics. Our study reveals a consistent picture of a smooth crossover centered at intermediate coupling ($U \approx 2 - 6$), characterized by the suppression of charge fluctuations, the formation of local moments, and a reduction in entanglement entropy. The spin-resolved charge gap exhibits a maximum in the gap difference between low- and high-spin sectors, signaling a non-trivial reorganization of spin correlations in the charge excitation spectrum. Local observables, including double occupancy and local moment, show the most rapid changes in the same interaction range, reinforcing the identification of this regime as the crossover region.

The application of PCA to charge and spin correlation matrices provides an unsupervised, data-driven view of the correlation reorganization. In the $S = 1/2$ sector, we observe a dramatic concentration of variance into a single principal component in the spin channel, indicating the emergence of a dominant antiferromagnetic fluctuation mode. In contrast, the $S = 3/2$ sector maintains a more distributed variance, reflecting the persistent frustration and absence of strong singlet formation. The spatial structure of the leading eigenvectors further illustrates the evolution from inhomogeneous metallic patterns to localized charge and staggered spin arrangements.

Complementing these measures, the quantum geometry distance matrices offers a wavefunction based perspective,

showing a clear transition from off-diagonal coherence to diagonal dominance as U increases. This geometric signature aligns with the other diagnostics and confirms the crossover in terms of the many-body localization of the wavefunction.

Overall, our multi-faceted approach consistently identifies the Mott crossover and highlights the significant differences between the $S = 1/2$ and $S = 3/2$ sectors. The $S = 1/2$ sector undergoes a sharper transition with well-developed antiferromagnetic correlations, while the $S = 3/2$ sector exhibits more gradual changes and retained frustration. These findings underscore the importance of spin sector in finite-size systems and provide a robust framework for characterizing correlation-driven crossovers in quantum materials.

-
- [1] N. F. Mott, Metal-insulator transitions, *Science* **188**, 1007 (1975).
 - [2] H. Park, K. Haule, and G. Kotliar, Cluster dynamical mean field theory of the mott transition, *Phys. Rev. Lett.* **101**, 186403 (2008).
 - [3] C. Hofrichter, L. Riegger, F. Scazza, M. Höfer, D. R. Fernandes, I. Bloch, and S. Fölling, Direct probing of the mott crossover in the SU(n) fermi-hubbard model, *Phys. Rev. X* **6**, 021030 (2016).
 - [4] Z. X. C. Y. e. a. Wu, F., Mott insulating phase and coherent-incoherent crossover across magnetic phase transition in 2d antiferromagnetic crsbr, *Sci. China Phys. Mech. Astron* **68**, 267411 (2025).
 - [5] M. Chatzieftheriou, S. Biermann, and E. A. Stepanov, Local and nonlocal electronic correlations at the metal-insulator transition in the two-dimensional hubbard model, *Phys. Rev. Lett.* **132**, 236504 (2024).
 - [6] M. F. Equbal, S. R. Hassan, and M. A. H. Ahsan, Exact diagonalization study of ground state properties and level statistics in simple and extended hubbard lattice cluster, *Physica Scripta* **100**, 035964 (2025).
 - [7] M. Imada, A. Fujimori, and Y. Tokura, Metal-insulator transitions, *Rev. Mod. Phys.* **70**, 1039 (1998).
 - [8] L. Wang, Discovering phase transitions with unsupervised learning, *Phys. Rev. B* **94**, 195105 (2016).
 - [9] N. C. Costa, W. Hu, Z. J. Bai, R. T. Scalettar, and R. R. P. Singh, Principal component analysis for fermionic critical points, *Phys. Rev. B* **96**, 195138 (2017).
 - [10] E. Khatami, Principal component analysis of the magnetic transition in the three-dimensional fermi-hubbard model, *Journal of Physics: Conference Series* **1290**, 012006 (2019).
 - [11] O. Vafek, N. Regnault, and B. A. Bernevig, Entanglement of exact excited eigenstates of the Hubbard model in arbitrary dimension, *SciPost Phys.* **3**, 043 (2017).
 - [12] Z. Xuan and T. Pei-Qing, Quantum phase transition and von neumann entropy of quasiperiodic hubbard chains, *Chinese Physics B* **17**, 1623 (2008).
 - [13] J. P. Coe, V. V. França, and I. D'Amico, Hubbard model as an approximation to the entanglement in nanostructures, *Phys. Rev. A* **81**, 052321 (2010).
 - [14] M. F. Equbal, S. R. Hassan, and M. A. H. Ahsan, Principal component analysis of ... hubbard models (2025), arXiv:2511.12551 [cond-mat.str-el].
 - [15] S. R. Hassan, R. Shankar, and A. Chakrabarti, Quantum geometry of correlated many-body states, *Phys. Rev. B* **98**, 235134 (2018).
 - [16] S. Acharya, B. Tellekamp, J. Jackson, D. Pashov, J. L. Blackburn, K. Alberi, and M. van Schilfgaarde, Origin of metal-insulator transition in rare-earth nickelates (2025), arXiv:2511.14960 [cond-mat.str-el].
 - [17] J. Hubbard, Electron correlations in narrow energy bands, *Proceedings of the Royal Society A* **276**, 238–257 (1963).
 - [18] C. R. Sarma and M. A. H. Ahsan, Electron correlation studies: Rumer basis approach, *International Journal of Quantum Chemistry* **60**, 147 (1996).